Available online at www.sciencedirect.com
SCIENCE DIRECT®
Journal of Photochemistry and Photobiology A: Chemistry 158 (2003) 111–117
Journal of Photochemistry and Photobiology A:Chemistry
www.elsevier.com/locate/jphotochem

Photoluminescence quenching of silicon nanoparticles in phospholipid vesicle bilayers

Heeun Jang [a], Lindsay E. Pell [b], Brian A. Korgel [b], Douglas S. English [a,*]

[a] *Department of Chemistry and Biochemistry, The University of Maryland, College Park, MD 20742, USA*
[b] *Department of Chemical Engineering, The University of Texas, Austin, TX 78712, USA*

Received 27 May 2002; received in revised form 2 September 2002; accepted 7 October 2002

Abstract

Due to its unique optical properties, nanostructured silicon is a promising material for optoelectronic applications, solar energy conversion and chemical sensors. This paper demonstrates the incorporation of organic-capped silicon nanoparticles into the hydrophobic interior of phospholipid vesicle bilayers, and uses photoluminescence quenching to determine the accessibility of membrane-embedded nanoparticles to aqueous and lipid-bound quenchers. Experiments with water-soluble quenchers indicate the existence of two populations of membrane-bound nanoparticles with varying accessibilities to the aqueous phase. Results from membrane-bound quenchers reveal that the major population localizes deep inside the bilayer. The ability of the nanoparticles to fully embed in the bilayer allows studies of their interactions with both aqueous and lipophilic molecules in a biomimetic environment. These composites may prove useful in the development of aqueous-based sensors and provide a model system for studying nanoparticle/cell interactions.

Keywords: Silicon nanoparticle; Quantum dot; Quenching; Vesicle; Bilayer

1. Introduction

Nanostructured silicon such as porous silicon (p-Si) [1], silicon nanoparticles [2–4] and nanowires [5] has spurred great interest due to the onset of strong visible photoluminescence (PL) as particle size decreases to the sub-10 nm scale. Above this limit, silicon exhibits the low PL intensities characteristic of indirect bandgap semiconductors in which the lowest-lying conduction band minimum occurs away from the Brillouin zone center [6,7]. For such materials to undergo a radiative electron–hole recombination requires participation of a phonon to preserve the total crystal momentum. This is a low probability event that precludes strong emission in silicon and other indirect bandgap materials such as Ge, SiC and GaP. For silicon crystallites below about 10 nm in dimension, radiative recombination becomes much more efficient and the bandgap widens dramatically. For instance crystallites on the 2–3 nm scale exhibit blue PL (∼3 eV) [3,8], well above the bulk silicon bandgap energy (E_g) of 1.1 eV [9].

Many applications have been proposed for nanoscale silicon including electro-optic devices [10], solar energy conversion [11] and chemical sensing applications [12,13]. Utilization of nanoscale silicon for sensing applications requires a basic understanding of its fundamental interactions with possible analytes. Toward this end many photophysical investigations have been carried out to study the interaction of porous silicon surfaces or oxide coated nanoparticles with various solutes in organic solutions. These studies have yielded interesting observations and measurements including chemical tunability by surface modification [14], steric sensitivity [15] and determination of bandgap [2,16]. This paper represents the first study of organic-capped silicon nanoparticles suspended in aqueous media by incorporation into the hydrophobic interior of a biomimetic membrane. Particles incorporated in the membrane retain their luminescent properties and can interact with molecules diffusing in the aqueous or lipid phase. This may have important implications toward the development of nanophase silicon-based devices useful in the detection of aqueous or lipid soluble analytes. Furthermore, the ability to trap the analyte in the confined environment of a bilayer will facilitate the so-called "sense and shoot" [17] approach in which analytes are simultaneously detected and destroyed by photo-initiated degradation. These bilayer/nanoparticle composites also provide a model system to study interactions of nanoparticles with cells and hydrophobic forces in lipid bilayers.

* Corresponding author. Tel.: +1-301-405-3368; fax: +1-301-314-9121.
E-mail address: de59@umail.umd.edu (D.S. English).

1010-6030/03/$ – see front matter © 2003 Elsevier Science B.V. All rights reserved.
doi:10.1016/S1010-6030(03)00024-8

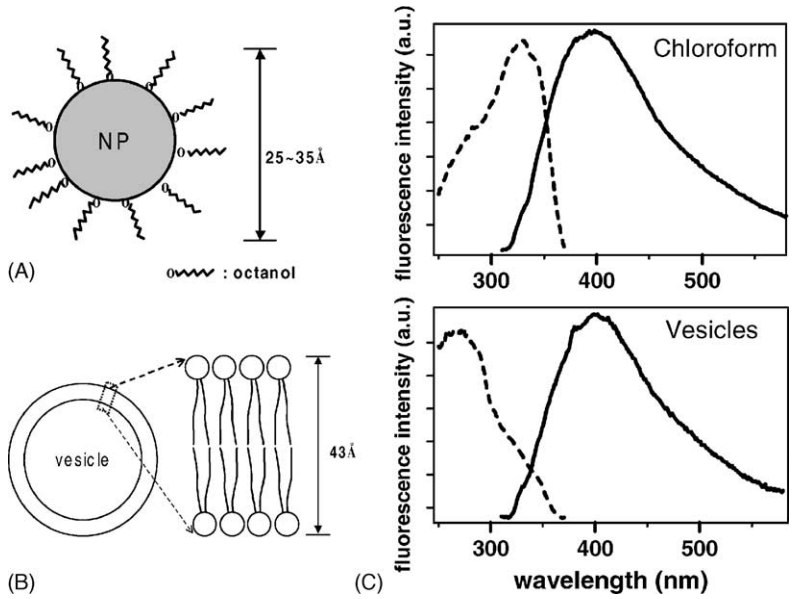

Fig. 1. (A) The nanoparticles in this study consist of a crystalline silicon core and a hydrophobic surface of organic capping ligands consisting of octanol chains. (B) Unilamellar vesicles ranging in size from 60 to 350 nm were used. The hydrophobic interior of the bilayer closely matches the size of the silicon nanoparticles facilitating the formation of a stable complex. (C) Excitation and emission spectra (dashed and solid lines, respectively) showing nanoparticles in chloroform and after incorporation in a lipid bilayer.

The nanoparticles used in these studies are capped with a monolayer of octanol in which the oxygen forms a covalent bond with the silicon nanocrystal surface, Fig. 1A. Previous reports have shown that these nanoparticles have efficient PL with size-tunable, discrete transitions and nanosecond lifetimes uncharacteristic of porous silicon or oxide coated nanoparticles [3,18]. The primary photophysical parameters are shown in Table 1. The very short PL lifetime of 2.6 ns is noteworthy since it is about 1000 times shorter than those reported previously for nanostructured silicon. Typical PL decay times for p-Si and oxide capped nanoparticles are in the microsecond range, though 70 ns decay times have been reported for blue emission from hydrogen passivated porous silicon nanoparticles [8]. These fast decay times and high quantum yields are believed to be the result of strong resonant mixing of the core and surface states [8,18]. The high quantum yields and reduced PL lifetimes have enabled detailed studies of single nanoparticles [18].

While surface chemistry appears to play an important role in the photophysics of these particles, the organic layer also provides steric stability during synthesis and hinders oxide formation at the nanocrystal surface. Furthermore, the capping ligands render the particles strongly hydrophobic making them insoluble in all but a few non-polar organic solvents. Given the size and hydrophobic exterior of these nanoparticles, they are excellent candidates for the formation of a stable complex with phospholipid-based unilamellar vesicles (Fig. 1B). Phospholipid membranes can provide a host matrix for many types of hydrophobic molecules such as cholesterol and proteins. The goal of this paper is to demonstrate the formation of nanoparticle/vesicle composites and provide structural information through optical interrogation of this new type of photofunctional material.

Table 1
Fundamental photophysical parameters of organic-capped silicon nanoparticles

ϕ_{PL}	0.05
τ_{PL} (ns)	2.6[a]
k_{rad} (s^{-1})	2.1×10^7
k_{nonrad} (s^{-1})	3.6×10^8

[a] The PL lifetime was actually fit to a sum of exponentials with an average lifetime of 2.6 ns, see Ref. [18] for details.

2. Experimental

2.1. Materials

2.1.1. Nanoparticle preparation

Organic-capped, crystalline silicon nanoparticles were prepared by decomposition of phenylsilane in supercritical octanol/hexane. This method is described in detail elsewhere [3]. Size exclusion chromatography using neutral, porous styrene divinylbenzene beads (Biobead S-X, Bio-Rad Laboratories Inc.) was used to select nanoparticles in the 2.5–3.5 nm range. The beads were dispersed in THF for column preparation and then flushed with chloroform before a sample was eluted.

2.1.2. Vesicle preparation

Egg yolk phosphatidylcholine (EYPC), 1-palmitoyl-2-stearoyl-16-DOXYL-sn-glycero-3-PC (16-DOXYL), and

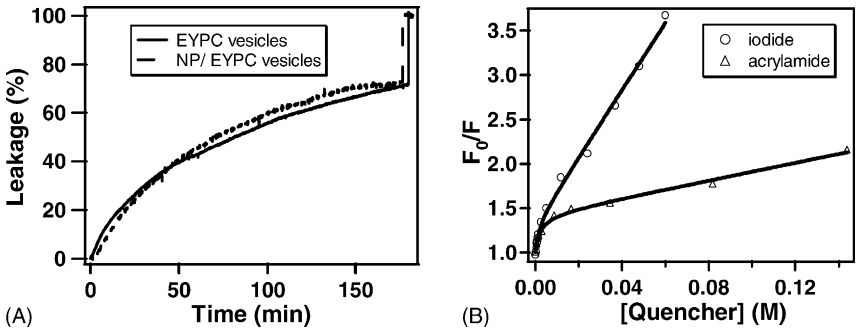

Fig. 2. (A) Results from efflux measurements using carboxyfluorescein in vesicles prepared with and without nanoparticles. (B) Quenching results for the water-soluble quenchers iodide and acrylamide.

1-palmitoyl-2-stearoyl-5-DOXYL-sn-glycero-3-PC (5-DOXYL), were purchased from Avanti Polar Lipids and used without further purification. Chloroform solutions of pure lipid or lipids with nanoparticles were dried with a gentle stream of nitrogen before drying overnight in a vacuum desiccator. The resulting films were hydrated with 1 ml of buffer (10 mM NaCl, 10 mM HEPES with 1 mM $Na_2EDTA{\cdot}2H_2O$ to reduce effects of trace cations) and drops of NaOH solution were added to attain a final pH of 7.5. Small unilamellar vesicles (60 nm diameter) were formed by sonication and larger vesicles (150 or 300 nm diameter) were formed by extruding 17 times using a polycarbonate membrane with 100 or 1000 nm pore size (Avanti Polar Lipids). Extrusion was preceded by five freeze-thaw cycles. Vesicle samples were purified using gel permeation chromatography (Sephadex G50, Amersham Pharmacia Biotech).

2.2. Procedures

2.2.1. Dynamic light scattering

DLS was carried out at 23 °C by measuring scattered laser light (HeNe $\lambda = 633$ nm) at 90° using a PMT (Photocor) and autocorrelator (Photocor 4.2.5). Vesicle samples from pure lipids and with nanoparticles were prepared and the effective hydrodynamic radii were measured. Results for extruded and sonicated vesicles are consistent with previous observations [19]. Vesicle size was also measured at acrylamide and iodide concentrations matching those used in the quenching experiments (see below).

2.2.2. Efflux measurements

Vesicles encapsulating carboxyfluorescein (50 mM) were prepared by the methods described by Rex [19]. Fluorescence from the encapsulated carboxyfluorescein is quenched by dye–dye interactions that are diminished as the dye leaks from the vesicle interior resulting in increased emission intensity. Dye filled vesicles or vesicle/nanoparticle composites were prepared and separated from free dye on a gel permeation column using Sephadex G50 (Amersham Pharmacia Biotech). The fresh sample was excited at 490 nm and the time dependent fluorescence intensity, $F(t)$, was monitored at 515 nm using a Fluorolog-3 fluorimeter (Jobin Yvon Horiba Inc.) with excitation and emission slits set to 3 nm resolution. Crossed polarizers were used to minimize the contribution of light scattering to the signal. The degree of efflux (dye leakage) was calculated by

$$\text{efflux}(t) = \frac{F(t) - F_0}{F_\infty - F_0} \quad (1)$$

where F_0 is the initial intensity and F_∞ was determined by inducing vesicle rupture with a drop of Triton-X solution after 3 h. Efflux progress was plotted for nanoparticle bearing vesicles and compared with control vesicles of pure lipid (Fig. 2A).

2.2.3. Aqueous quencher experiments

Nanoparticle bearing EYPC vesicles were made in buffer by extrusion. Nanoparticles were excited at 325 nm. A 5 nm bandpass was used for excitation while 1 nm resolution was used for emission. Crossed excitation and emission polarizers were employed to decrease contributions from scattered light. Acrylamide and iodide were used as aqueous-based quenchers and Stern-Volmer plots were constructed. Stern-Volmer plots constructed using integrated intensity correspond well with those in which peak intensities were used to calculate quenching. Pure EYPC vesicles were used to collect scattering background for correction. Fresh NaI solution was used within 3 h after preparation to avoid I_3^- formation.

2.2.4. Spin-label quencher experiments

The nanoparticle/EYPC/DOXYL lipid films were prepared with ratios of EYPC:DOXYL of 1:10 and 1:5, spin-label concentration were determined from absorption spectra taken in chloroform and using $\varepsilon_{420\,\text{nm}} = 5\,\text{M}^{-1}\,\text{cm}^{-1}$ [20]. Two spin-labeled lipids were used, 5- and 16-DOXYL, see Fig. 3. Vesicles from EYPC only were also made as a control. Vesicles were made by sonication in buffer. PL was collected with excitation at 325 nm and crossed polarizers were used. Spectra of each sample were measured after storage for 18 h at 8 °C to check the stability of the nanoparticles in the bilayer over time.

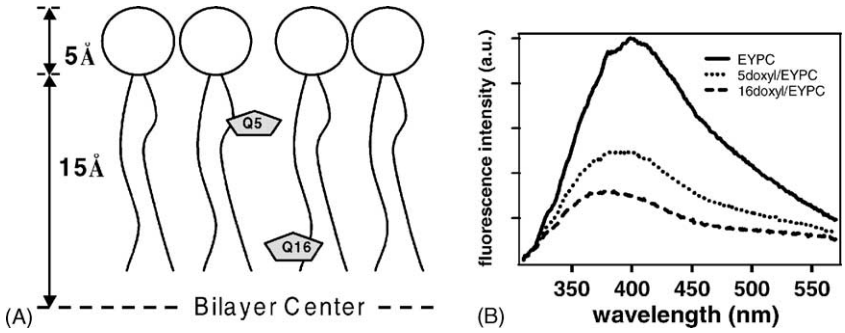

Fig. 3. (A) Schematic depiction of quencher depths for 5- and 16-DOXYL. (B) Comparison of emission spectra of nanoparticles in vesicles prepared from EYPC and with 5- and 16-DOXYL.

3. Results

Multiple spectroscopic methods were employed to determine the nature of the nanoparticle/bilayer interactions and the resulting complex. These included dynamic light scattering, PL quenching, spin-label quenching, and efflux measurements. Perhaps the most compelling evidence that the nanoparticles are indeed partitioning to the bilayer of individual vesicles comes from the use of gel permeation chromatography. After samples were prepared they were passed through a gel permeation column packed with Sephadex G50. This particular resin is commonly used to separate vesicles from extravesicular molecules, and individual nanoparticles or small clusters of nanoparticles and lipid molecules would fall within the fractionation range of this media (1500–30,000 for globular proteins). For these samples, vesicles elute from the column in a distinct band while smaller structures and impurities exhibit a longer retention time. Excitation and emission spectra from the vesicle band are shown in Fig. 1C. The vesicle band always exhibits nanoparticle emission, providing direct evidence that the nanoparticles and vesicles are strongly associating.

3.1. Dynamic light scattering and efflux measurements

Dynamic light scattering experiments were used to measure the effects of nanoparticle incorporation on the size and stability of the vesicle samples. Additional measurements were carried out over the range of quencher concentrations to ensure that the vesicles remained intact during the quenching experiments. During these experiments, it was noted that initial vesicle volume was reduced by 30% after the first addition of iodide (5 mM) and continued to decrease to 44% at the final concentration of 65 mM. Similarly for acrylamide the initial decrease in volume was 31% with a final volume of 42%. The shrinking of vesicles due to sharp changes in osmotic pressure is a well-known phenomena [21].

Efflux measurements [22] were used to monitor the membrane permeability to the entrapped, self-quenching dye, carboxyfluorescein. No significant change in membrane permeability was detectable when results from vesicles containing membrane-bound nanoparticles were compared with those from pure EYPC vesicles (Fig. 2A). This suggests that the nanoparticle interactions with the bilayer do not induce significant local disorder which would lead to increased bilayer permeability.

3.2. PL quenching with aqueous-based quenchers

PL quenching experiments employing water-soluble quenchers were used to determine the accessibility of the membrane-bound nanoparticles to the aqueous phase. Similar approaches have been used to study the photophysics, surface chemistry and electronic structure of nanostructured silicon samples [2,14,16,23–25]. It has been shown that certain quenchers act as either conduction or valence band quenchers through transfer of an electron or hole from Si to the quencher [2,16]. The studies reported here employ quenchers with minimal solubility in the non-polar region of the bilayer [26]. Quenching of silicon was observed over a range of concentrations and standard Stern-Volmer plots were made.

The Stern-Volmer plots for acrylamide and iodide quenching are displayed in Fig. 2B. The salient feature of these plots is their strong deviation from linearity predicted by the Stern-Volmer equation:

$$\frac{I_0}{I_Q} = 1 + k_{SV}[Q] = 1 + k_Q\tau_0[Q] \quad (2)$$

where I_0 and I_Q are unquenched and quenched PL intensity, respectively; $[Q]$ the quencher concentration; k_{SV} the Stern-Volmer quenching constant and is the product of the unquenched PL lifetime and a bimolecular rate constant $[k_Q]$ describing collisional quenching. The bimolecular rate constant can be thought of as the rate of collisions (k_0) multiplied by an effective reaction efficiency: $k_Q = k_0\sigma$.

Strong deviation from linearity like that displayed in Fig. 2B is sometimes observed in quenching experiments involving proteins [27,28] and has been predicted by theory for fluorophores in micelles and vesicles [29]. The negative curvature of the Stern-Volmer plot is interpreted as a result of two nanoparticle populations. This is a standard

interpretation that has been successfully applied to analyze the quenching data of proteins and peptides with multiple conformations and/or multiple tryptophans [27,28].

If the emission is assumed to arise from two populations of fluorophores, one more accessible and the other less accessible with identical PL spectral shapes and quantum yields, then the total fluorescence (F_0) is the sum of the fluorescence from the two populations a and b:

$$F_0 = F_a + F_b \tag{3}$$

From Eqs. (2) and (3), the total fluorescence in the presence of quenchers may be written as

$$F_Q = \frac{f_a F_0}{1 + k_{qa}\tau_0[Q]} + \frac{(1 - f_a)F_0}{1 + k_{qb}\tau_0[Q]} \tag{4}$$

where $f_a = F_a/(F_a + F_b)$. Eq. (4) yields

$$\frac{F_0}{F_Q} = \left(\frac{f_a}{1 + k_{qa}\tau_0[Q]} + \frac{(1 - f_a)}{1 + k_{qb}\tau_0[Q]}\right)^{-1} \tag{5}$$

The quenching curves for the silicon nanoparticles (Fig. 2B) were fit to equation [5] and the fitted parameters are shown in Table 2. There are several important points which warrant elaboration. First the fastest rate constant, k_a, is significantly greater than that which is expected for a diffusion limited reaction between a freely diffusing nanoparticle ($r = 1.5$ nm) and a quenching molecule given by

$$k_0 = \frac{4\pi NDR}{1000} \tag{6}$$

where N is the Avogadro's number, D the sum of the diffusion coefficients for nanoparticle and quencher and R the sum of their radii. This value is expected to be, approximately, $1.5 \times 10^{10}\,M^{-1}\,s^{-1}$ for acrylamide and iodide. Second, the similarity of the value determined for f_a from both the iodide data (0.27) and the acrylamide data (0.30) is important since this value should be independent of the quencher used, assuming that the two quenchers have similar partitioning to the bilayer interior. Finally, iodide shows a more efficient quenching rate than acrylamide for both nanoparticle populations. Strong quenching by iodide relative to acrylamide has been reported for other membrane-embedded fluorophores [26].

3.3. PL quenching from membrane-bound, spin-label quenchers

The results obtained by using aqueous-based quenchers, size exclusion chromatography and from DLS measurements are all consistent with the existence of membrane-bound nanoparticle populations of varying accessibility to the extravesicular aqueous phase. The efflux measurements indicate that the bilayer permeability is not significantly affected by nanoparticle incorporation. This result suggests a weak or non-perturbing interaction between the nanoparticle and vesicle bilayer possibly from the shallow embedding of nanoparticles in one leaflet without spanning the entire bilayer. In order to test this model covalently linked quenchers located at the 5 (near the head-group) and 16 (at the acyl chain end) positions of the lipid tail groups were employed to measure the membrane penetration depth (Fig. 3A). This technique was developed by Chattopadhyay and London [30] and has been used to successfully measure the position and orientation of membrane spanning chromophore [31].

Table 2
Fitted parameters from Eq. (5)

	Iodide	Acrylamide
ϕ_a	0.27	0.30
k_{qa} ($M^{-1}\,s^{-1}$)	2.05×10^{11}	1.59×10^{11}
k_{qb} ($M^{-1}\,s^{-1}$)	6.95×10^{9}	8.65×10^{8}
k_0 ($M^{-1}\,s^{-1}$) (from Eq. (6))	1.68×10^{10}	1.51×10^{10}

The degree of penetration can be inferred from the relative efficiency of quenching from the two differently located quenchers. Fig. 3B shows the PL intensity for silicon nanoparticles in pure EYPC vesicles, and in the presence of 5- and 16-labeled lipids. The relative intensity is $(F_{16\text{-lablel}})/(F_{5\text{-label}}) = 0.7$. This indicates that the nanoparticles are localized in close proximity to the *acyl chain ends* and therefore must be deeply imbedded in the bilayer.

4. Discussion

The incorporation of nanoparticles into vesicle bilayers is evinced by the appearance of strong nanoparticle emission from the vesicle band during gel permeation chromatography (Fig. 1C). DLS data shows that nanoparticle incorporation does not significantly affect the vesicle size or stability. These results could be anticipated considering that biological membranes are highly heterogeneous structures with a variety of hydrophobic molecules existing in and across their hydrophobic interior. The incorporation of hydrophobic-capped nanoparticles into a lipid bilayer is similar to the inclusion of integral membrane spanning proteins in natural biological membranes. In the formation of protein–bilayer complexes the perturbed lipid molecules surrounding the protein are known as the *boundary lipids* and, in the case of a mixed bilayer, may have a distinct chemical composition different from the unperturbed bilayer. In the case of a pure (single lipid) bilayer system, the boundary lipids are typified by unique geometric constraints, which can include tilt and stretching or compressing of the flexible acyl chains. To a first approximation these effects can be described by an effective elastic energy, the energy required for a boundary lipid to accommodate a protein of hydrophobic region length (L) [32]. The elastic energy per lipid molecule is given by

$$E_{el} = \frac{1}{2}\kappa^{-1}\left(\frac{L - l}{l}\right)^2 A \tag{7}$$

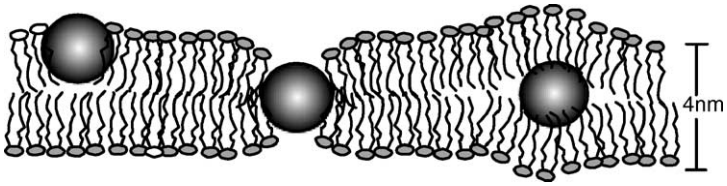

Fig. 4. Sketches of possible nanoparticle/bilayer interactions.

In this case $L = 2r$, where r is the nanoparticle radius. The parameter κ is the lateral compressibility, l the lipid chain length (i.e. half the length of hydrophobic region), and A the surface area per lipid molecule. Using $\kappa = 20$ m/N [33], $l = 1.5$ nm [34], $A = 0.7\,\text{nm}^2$ [35] and $L = 3$ nm gives $E_{el} = 1.7 \times 10^{-20}$ J or about 4 kT at 298 K (4.1×10^{-21} J). It is instructive to compare E_{el} with the free energy change associated with the transfer of the alkyl capping ligands from water to the hydrophobic bilayer interior. The net free energy change for removal of a methylene group from water to a polar environment is negative and on the order of 5×10^{-21} J [21]. Clearly the removal of several octane chains from water to the lipid bilayer would provide the thermodynamic driving force to overcome the energy needed to distort the bilayer.

Even after size selection chromatography, there exist size and shape variations of individual nanoparticles. As a result, there will be a range of penetration depths and interactions between the nanoparticles and bilayer. The quenching data shown in Fig. 2 is representative of data for multiple populations of fluorophores with varying accessibility by the quencher molecules. Table 2 shows that approximately one-third of the nanoparticles undergo very efficient quenching. This population may represent nanoparticles with shape, size or surface chemistry which is not compatible to deep penetration in the bilayer. However, comparisons between Stern-Volmer plots constructed from either integrated or peak PL intensities show that there is not selective quenching of a specific spectral region that would suggest a purely size dependent effect. The value for k_{aq} exceeds the diffusion limit and can be interpreted as evidence for formation of a highly quenched complex of the nanoparticle with quencher molecules. It should be noted that the formation of a highly quenched and stable complex is a desirable property for applications in chemical sensing and would enhance detection limits. It should also be noted that the unexpectedly large value of k_{aq} may arise from diffusion of adsorbed quenchers on the vesicle surface. Reactions between surface adsorbed species on micelles and vesicles have accelerated reaction rates that are readily modeled by application of a mean reaction time approximation for a pair of diffusing particles on a spherical surface [36]. In contrast to the large values observed for k_{aq}, the values for k_{bq} are consistent with diffusional quenching. A distinctly higher rate is observed for iodide than for acrylamide. This discrepancy in quenching efficiency has been noted for membrane-bound fluorophore and cannot be explained by disparity in permeation coefficients between acrylamide and iodide, since they are similar.

Based on evidence from efflux measurements and diffusive quenching one might speculate that nanoparticle interactions with the bilayer are weak and non-perturbing, suggesting a partial embedding of the nanoparticle in the lipid bilayer. Results from spin-label quenching measurements, however, are not consistent with this hypothesis. In these quenching experiments two quenchers were used. One quencher (5-DOXYL) was labeled near the head-group and the other was labeled at the acyl chain end (16-DOXYL). There are three possible outcomes from these experiments:

(i) Similar quenching observed for both lipids.
(ii) Greater quenching from 5-DOXYL.
(iii) Greater quenching from 16-DOXYL.

The first result (i) would indicate a structure in which a nanoparticle spans the hydrophobic region making equivalent contact with the two quencher populations. The second result (ii) would indicate that the nanoparticles were only partially embedded in the bilayer or resting on the vesicle surface. The third result (iii), the one which was observed, indicates that the bilayer envelopes the nanoparticle as shown on the right in Fig. 4 since spanning of the bilayer would presumably result in roughly equivalent quenching from 5- and 16-DOXYL. The fact that stronger quenching was observed for 16-DOXYL is unequivocal evidence that a significant portion of the nanoparticles are deeply embedded in the bilayer.

5. Conclusions

Bilayer encapsulation offers a convenient means to measure nanoparticle interaction with both aqueous and lipid-based quenchers. The combined results from quenching by water-soluble molecules and spin-labeled lipids point to a heterogeneous distribution of nanoparticles partitioning to varying depths in the lipid bilayer. Sketches of some hypothetical structures are displayed in Fig. 4. While these structures are consistent with quenching data more direct measurements such as freeze-fracture or cryogenic transmission electron microscopy will be needed for definitive determination. Potential applications for these composite materials include aqueous-based chemical sensors and model systems for hydrophobic interactions.

Acknowledgements

The authors would like to thank Darryl Williams for assistance with the light scattering measurements and Robert Walker for the generous use of his fluorimeter.

References

[1] L.T. Canham, Silicon quantum wire array fabrication by electrochemical and chemical dissolution of wafers, Appl. Phys. Lett. 57 (1990) 1046–1048.
[2] I.N. Germanenko, S. Li, M.S. El-Shall, Decay dynamics and quenching of photoluminescence from silicon nanocrystals by aromatic nitro compounds, J. Phys. Chem. B 105 (2001) 59–66.
[3] J.D. Holmes, K.J. Ziegler, R.C. Doty, L.E. Pell, K.P. Johnston, B.A. Korgel, Highly luminescent silicon nanocrystals with discrete optical transitions, J. Am. Chem. Soc. 123 (2001) 3743–3748.
[4] L.E. Brus, P.F. Szajowski, W.L. Wilson, T.D. Harris, S. Schuppler, P.H. Citrin, Electronic spectroscopy and photophysics of Si nanocrystals—relationship to bulk c-Si and porous Si, J. Am. Chem. Soc. 117 (1995) 2915–2922.
[5] J.D. Holmes, K.P. Johnston, R.C. Doty, B.A. Korgel, Control of thickness and orientation of solution-grown silicon nanowires, Science 287 (2000) 1471–1473.
[6] S.S. Lyer, Y.-H. Xie, Light emission from silicon, Science 260 (1993) 40–46.
[7] J.I. Pankove, Optical Processes in Semiconductors, Dover, New York, 1971.
[8] M.V. Wolkin, J. Jorne, P.M. Fauchet, G. Allan, C. Delerue, Electronic states and luminescence in porous silicon quantum dots: the role of oxygen, Phys. Rev. Lett. 82 (1999) 197–200.
[9] M.L. Cohen, T.K. Bergstresser, Band structures and pseudopotential form factors for fourteen semiconductors of the diamond and zinc-blende structures, Phys. Rev. 141 (1966) 789–796.
[10] K.D. Hirschman, L. Tsybeskov, S.P. Duttagupta, P.M. Fauchet, Silicon-based visible light-emitting devices integrated into microelectronic circuits, Nature 384 (1996) 338–341.
[11] V. Pacebutas, K. Grigoras, A. Krotkus, Porous silicon applications in solar cell technology, Phys. Scripta T 69 (1997) 255–258.
[12] M.T. Kelly, A.B. Bocarsly, Mechanisms of photoluminescent quenching of oxidized porous silicon—applications to chemical sensing, Coord. Chem. Rev. 171 (1998) 251–259.
[13] S. Content, W.C. Trogler, M.J. Sailor, Detection of nitrobenzene, dnt, and tnt vapors by quenching of porous silicon photoluminescence, Chem.-Eur. J. 6 (2000) 2205–2213.
[14] J.M. Lauerhaas, M.J. Sailor, Chemical modification of the photoluminescence quenching of porous silicon, Science 261 (1993) 1567–1568.
[15] R.R. Chandler-Henderson, B. Sweryda-Krawiec, J.L. Coffer, Steric considerations in the amine induced quenching of luminescent porous silicon, J. Phys. Chem. 99 (1995) 8851–8855.
[16] J.M. Rehm, G.L. McLendon, P.M. Fauchet, Conduction and valence band edges of porous silicon determined by electron transfer, J. Am. Chem. Soc. 118 (1996) 4490–4491.
[17] P.V. Kamat, R. Huehn, R. Nicolaescu, A sense and shoot approach for photocatalytic degradation of organic contaminants in water, J. Phys. Chem. B 106 (2002) 788–794.
[18] D.S. English, L.E. Pell, Z. Yu, P.F. Barbara, B.A. Korgel, Size tunable visible luminescence from individual organic monolayer stabilized silicon nanocrystal quantum dots, Nano Lett. 2 (2002) 681–685.
[19] S. Rex, Pore formation induced by the peptide melittin in different lipid vesicle membranes, Biophys. Chem. 58 (1996) 75–85.
[20] S.E. Herbelin, N.V. Blough, Intramolecular quenching of excited singlet states in a series of fluorescamine-derivatized nitroxides, J. Phys. Chem. B 102 (1998) 8170–9176.
[21] M.K. Jain, Introduction to Biological Membranes, Wiley, New York, 1988.
[22] J.N. Weinstein, S. Yoshikami, P. Henkart, R. Blumenthal, W.A. Hagins, Liposome-cell interaction—transfer and intracellular release of a trapped fluorescent marker, Science 195 (1977) 489–492.
[23] M.T. Kelly, J.K.M. Chun, A.B. Bocarsly, A silicon sensor for so2, Nature 382 (1996) 214–215.
[24] M.C. Ko, G.J. Meyer, Dynamic quenching of porous silicon photoluminescence by anthracene and 10-methylphenothiazine, Chem. Mater. 7 (1995) 12–14.
[25] D. Andsager, J. Hilliard, J.M. Hetrick, L.H. Abuhassan, M. Plisch, M.H. Nayfeh, Quenching of porous silicon photoluminescence by deposition of metal adsorbates, J. Appl. Phys. 74 (1993) 4783–4785.
[26] F. Moro, F.M. Goni, M.A. Urbaneja, Fluorescence quenching at interfaces and the permeation of acrylamide and iodide across phospholipid bilayers, FEBS 330 (2) (1993) 129–132.
[27] D.S. English, R.L. Rich, J.W. Petrich, Nonexponential fluorescence decay of 7-azatryptophan induced in a peptide environment, Photochem. Photobiol. 67 (1998) 76–83.
[28] R. Swaminathan, N. Periasamy, J.B. Udganokar, G. Krishnamoorthy, Molten globule-like conformation of barstar: a study of fluorescence dynamics, J. Phys. Chem. 98 (1994) 9270–9278.
[29] M. Tachiya, Stochastic and diffusion models of reactions in micelles and vesicles, in: G.R. Freeman (Ed.), Kinetics of Nonhomogeneous Processes, Wiley, New York, 1987.
[30] A. Chattopadhyay, E. London, Parallax method for direct measurement of membrane penetration depth utilizing fluorescence quenching by spin-labeled phospholipids, Biochemistry 26 (1987) 39–45.
[31] B. Ghebremariam, V. Sidorov, S. Matile, Direct evidence for the importance of hydrophobic mismatch for cell membrane recognition, Tetrahedron Lett. 40 (1999) 1445–1448.
[32] K.A. Fisher, W. Stoeckenius, Membranes, in: W. Hoppe, W. Lohman, H. Markl, H. Ziegler (Eds.), Biohphysics, Springer, Berlin, 1983.
[33] T. Heimburg, D. Marsh, Thermodynamics of the interaction of proteins with lipid membranes, in: K. Merz, B. Roux (Eds.), Biological Membranes, Birkhauser, Boston, 1996.
[34] J.N. Israelachvili, Intermolecular and Surface Forces, Academic Press, San Diego, 1992.
[35] B.A. Lewis, D.M. Engelman, Lipid bilayer thickness varies linearly with acyl chain-length in fluid phosphatidylcholine vesicles, J. Mol. Biol. 166 (1983) 211–217.
[36] H. Sano, M. Tachiya, Theory of diffusion-controlled reactions on spherical surfaces and its application to reactions on micellar surfaces, J. Chem. Phys. 75 (1981) 2870–2878.